journal

J. Am. Ceram. Soc., 88 [6] 1427–1434 (2005)
DOI: 10.1111/j.1551-2916.2005.00322.x

Model for Sintering Devitrifying Glass Particles with Embedded Rigid Fibers

M. J. Pascual and A. Durán†

Instituto de Cerámica y Vidrio (CSIC), Campus de Cantoblanco, 28049 Madrid, Spain

M. O. Prado

Centro Atómico Bariloche, Comisión Nacional de Energía Atómica, 8400-SC de Bariloche, RN, Argentina

E. D. Zanotto

Department of Materials Engineering-DEMa, Federal University of São Carlos-UFSCar 13565-905, São Carlos, SP, Brazil

We extend the *Clusters* model to account for the presence of rigid inclusions and use it to analyze the experimental sintering kinetics of composites of $60SiO_2 \cdot 24B_2O_3 \cdot 16Na_2O$ glass particles and zirconia fibers. We followed the densification kinetics of such composites as a function of the particle size, volume fraction of fibers, fiber to pore size ratio, temperature, and time of thermal treatment. The parameters of the extended *Clusters* model are the glass particle size distribution and shape factor, the fiber volume fraction and radii, the glass viscosity and surface tension, the number of nucleating sites per unit surface, and the crystal growth rate in the parent glass. Hydrostatic tensions caused by the fibers were also included in the calculations. The modified *Clusters* model with only one adjustable parameter, which is largely dominated by viscosity but also includes particle shape, allowed us to account for the effect of surface crystallization and fiber content as inhibitors of densification and successfully describe the sintering kinetics of the studied composites.

Nomenclature

Fk = Frenkel regime of sintering
MS = Mackenzie–Shuttelworth regime of sintering

Parameters of the composite:
r_f = average fiber radius (m)
f = actual fiber volume not including the porosity among fibers (m^3)
$\breve{\mathbf{f}}$ = volume of the pores among fibers (m^3)
$F = f + \breve{\mathbf{f}}$ (m^3)
g = glassy volume of the regions that only include glass–glass contacts (m^3)
$\breve{\mathbf{g}}$ = volume of pores associated to volume g (m^3)
$G = g + \breve{\mathbf{g}}$ (m^3)
g' = glassy volume of the regions that only include glass–fiber contacts (m^3)
$\breve{\mathbf{g}}'$ = volume of pores associated to volume g' (m^3)
$G' = g' + \breve{\mathbf{g}}'$ (m^3)
ρ_f = fiber density (kg/m^3)
$\rho(t)$ = relative density of volume G, calculated with the *Clusters* model ($\rho(0) = \rho_0$)
$\rho_c(t)$ = relative density of the composite (glass, fibers, porosity)
ρ_{th} = theoretical density of the composite, without porosity (kg/m^3)
p_f = number of neighbors per particle

Physical properties of the glass:
ρ_g = actual glass density (kg/m^3)
$\eta(T)$ = glass viscosity ($Pa \cdot s$)
γ = glass/vapor surface tension (J/m^2)

Crystallization parameters:
$U(T)$ = crystal growth rate (m/s)
$N_s(t)$ = density of surface nucleation sites ($N_s = N_s^0 + I_s t$) (m^{-2})
N_s^0 = density of surface nucleation sites at $t = 0$ (m^{-2})
I_s = surface nucleation rate ($m^{-2} \cdot s^{-1}$)

I. Introduction

(1) Literature Review

Powder processing of ceramic matrix composites has been thoroughly reviewed, with emphasis on forming powder compacts containing fiber reinforcement.[1] That work explains the importance of the relative size of the fibers and sintering particles.

Rigid (non-sintering) inclusions always retard the densification of a sintering body creating hydrostatic tensile stresses in the matrix[2] that can also produce defects, such as cracks.[3,4] Some authors have tried to analytically determine the stresses developed during sintering and their effect on densification.[5–8] For instance, it was shown that the number of spherical mono-sized inclusions (***n***) uniformly distributed in a powder compact influences the early stages of sintering. The hydrostatic tensile stress increases and the sintering rate decreases with the increase of ***n***.

Scherer[9] modeled the effect of such inclusions on sintering and applied the theory for the case of viscous sintering. Two models were considered. In the first, the composite was represented as one sphere having a central inclusion surrounded by a viscous matrix. This model has been used by other authors[5–8] and can be applied to low volume fractions of inclusions, where the fields of tensions around the inclusions do not overlap. The second model involves a compact constituted of a bimodal particle size distribution.[10] This model, denominated "self-consistent model," can be applied up to the point where the inclusion volume fraction is so great that a continuous network is formed and suppresses the contraction of the composite material. For the case of viscous sintering, the predictions of both models are indistinguishable for inclusion of volume fractions lower than 0.2. Subsequently, Scherer[11] used the self-consistent model to

G. W. Scherer—contributing editor

Manuscript No. 10037. Received March 12, 2003; approved December 28, 2004.
This work was partially funded by the Cyted network VIII.E and project VIII.10 (CNPq/Cyted), the research project CICYT MAT 2003-05902-C02-01 (Spain), and Integrated Action CSIC/CNPq (2004Br0011).
†Author to whom correspondence should be addressed. e-mail: aduran@icv.csic.es

describe viscous sintering of a material having an arbitrary distribution of pores in the presence of rigid inclusions.

Rahaman and De Longhe[6] carried out an experimental study of densification of soda-lime glass compacts containing different volume fractions of silicon carbide particles. The authors found good agreement between the experimental densification rates and those predicted by the rule of mixtures for silicon carbide volume fractions ≤ 0.1. The data for the densification rates and the stresses caused by the inclusions were in excellent agreement with the Scherer theory for volume fractions ≤ 0.12. These results suggest that it is possible to obtain composites of high density by means of conventional (pressureless) viscous flow sintering for volume fractions ≤ 0.15.

Dutton and Rahaman[7] studied the sintering, creep, and electrical conductivity of model vitreous matrix composites as a function of the content and size of inclusions. The composites were formed by spherical particles of soda-lime glass and spherical nickel inclusions. The authors did not observe any effect of the inclusion size on viscosity for volume fractions below 10%. Above this value, they claim there is an effect of the inclusion size with an important increase of viscosity because of the interaction between inclusions. The sintering rates were compared with the predictions of the self-consistent model of Scherer.[11] Good agreement was found when the creep viscosity was used in the model equation.

Boccaccini[8] studied the effect of Al_2O_3 platelets on the pressureless densification of an aluminosilicate glass. Both the creep rates and the hydrostatic stresses, calculated by the Scherer model, were in good agreement with the experimental results.

Raj and Bordia[3] developed a different approach to the problem of inhomogeneous sintering, in which deformation flow and densification are described with simple expressions. The maximum tensile stress generated by incompatible sintering between glass and inclusions was found to be sensitive to the ratio, β, of the rate constant for creep to the rate constant for densification, and depends mainly on the viscosity of the glass matrix and the volume fraction of inclusions. A large value of β implies a low magnitude of stress. The generation of flaws as a result of this stress was considered. These authors obtained solutions for the average contraction rate and the interfacial stress of the composite and demonstrated that, unless β is large, the densification rate of the composite will deviate significantly from the rule of mixtures.

Although these models are rather complex, they do not apply to the common case where the glass particles partially crystallize during sintering, arresting viscous flow and imparting densification. The influence of crystallization is then an additional (complex) problem. Panda *et al.*[12,13] made one of the first attempts to analyze the relative rates of sintering and crystallization of some glasses.

(2) Objective

The incorporation of zirconia fibers into a borosilicate glass matrix increases the corrosion resistance against molten carbonates and improves the mechanical properties of the system without significantly modifying the thermal expansion of the glass matrix, thus improving the sealing characteristics for use in molten carbonate fuel cells. In a previous study, Pascual *et al.*[14] investigated the sintering behavior of mixtures of a borosilicate glass and ZrO_2 fibers as a function of the particle size of the glass powder, sintering temperature, and time, in order to optimize sealing properties. The experimental sintering results were analyzed by using different sintering models for a glass matrix containing rigid inclusions, such as Scherer's model and the model of Raj and Bordia.[3,9,11,15] The sintering results did not fit any of those two sintering models because they do not consider the size and geometry of the inclusions and the effect of glass crystallization during sintering.

In this work, we present a new approach for modeling the sintering behavior of crystallizable glass powders having rigid inclusions. We analyze the sintering kinetics of the same borosilicate glass/ZrO_2 fiber system using a modified form of the *Clusters* model.[16] This model considers the sintering kinetics of a certain size distribution of glassy particles as the weighed sum of the sintering kinetics of each particle size[16] and takes into account densification with simultaneous crystallization, which was discussed at length in Zanotto and Prado[17] and Prado *et al.*[18,19]

(3) Theory

We consider that the volume fraction of a composite that only exhibits glass–glass contacts among particles will sinter as a conventional compact of glass particles. According to the *Clusters* model, the following expressions can describe the isothermal sintering kinetics of a powder compact in the absence of crystallization.

For each particle size, the overall sintering kinetics are described by two models. For $\rho < 0.8$, the Frenkel model is used (Eq. (1*a*), $\rho \leq 0.8$), and for $\rho > 0.8$, the Mackenzie–Shuttleworth model is used (Eq. (1*a*), $\rho > 0.8$). For each particle size:

$$\rho(r,t) = \rho_0\left(1 - \frac{Ct}{\eta(T)}\right)^{-3}, \rho \leq 0.8 \text{ and } \rho > 0.8$$
$$\rho(t) = 1 - (1-\rho_0)e^{-(C't/\eta(T))} \quad (1a)$$

where ρ_0 is the relative green density of the glass compact, $\eta(T)$ is the glass viscosity, $C = 3\gamma/8r$ and $C' = 3\gamma/2a_0$, γ is the glass–vapor surface energy, and a_0 is the pore radius at $t = 0$.

For each particle size, a value of a_0 is calculated so that at $t = t_{0.8}$, $\rho_{Fk}(t_{0.8}) = \rho_{MS}(t_{0.8})$. We will denominate ρ_{Fk} as the density given by the Frenkel model and ρ_{MS} as the density given by the Mackenzie–Shuttleworth model. $\theta(t_0 - t)$ is a step function that is unity when the argument is positive ($t < t_0$), and zero otherwise. Then, for a size distribution of particles, with a volume fraction v_r of particles of size r, the density can be expressed as

$$\rho(t) = \sum_r [\rho_{Fk}(r,t)\theta(t_{0.8} - t) + \rho_{MS}(r,t)\theta(t - t_{0.8})]v_r \quad (1b)$$

Equation (1*b*) sums the relative density, $\rho(r,t)$, for each particle size, r, as a function of time, t.

When dealing with large size distributions, we proposed[16] that, during the Frenkel stage, the volume fractions must be weighted according to their neck-forming ability, ξ_r, but this correction is not necessary in the present case. It was also proposed[20] that the average number of neighbors of each particle in the green compact must be considered, but as, in this case, this value is unknown; we express ρ_{Fk} as in Eqs. (1*a*) and (1*c*), where a cubic array is assumed for the glass particle compact. Otherwise, a packing factor, p_f, equal to the actual average number of neighbors divided by six should be used.

Equation (1*a*) was developed for spherical particles. Although it has been noticed that the sintering kinetics of irregular particles may differ from those of spherical particles, as far as we know, there is not yet a theoretical solution for such a complex problem. Thus, in practice, an empirical shape factor, k_s, is introduced in the calculation of $\rho_{Fk}(r,t)$. The use of k_s was discussed in Prado *et al.*[21] Usually $k_s > 1$ for irregular particles, but this value also depends on the particle packing. Improved packing resulting from, for example, a wider particle size distribution or use of lubricants generates a larger number of necks among particles per unit volume, leading to faster sintering kinetics. If one is not aware of this fact, it is possible that this effect is assigned to a shape factor larger than 1. Throughout this paper, we will assume $k_s = 1$; it will not, therefore, appear in the equations and will be included in the fitted value of viscosity (to be discussed later in this article).

Moreover, if the glass devitrifies with a surface density of nucleation sites, N_s, and crystal growth rate, $U(T)$, the inhibiting effect of crystallization on sintering must be included. In this work, we take the derivations of Zanotto and Prado,[17] which

model isothermal sintering with simultaneous crystallization, as shown by the following equations. These equations describe the sintering kinetics with simultaneous surface crystallization of the regions where only glass–glass contacts are present:

$$\rho_{Fk}(t) = \rho_0 + \frac{3C\rho_0}{\eta} H \int_0^t \left(1 - H\frac{Ct'}{\eta}\right)^{-4} \times e^{-\pi[N_s^0 U^2 t'^2 + I_s U^2 t'^3/3]}\, dt' \quad (1c)$$

$$\rho_{MS}(t) = \rho_0 + (1-\rho_0)\frac{C'}{\eta(\text{effective})} \int_0^t e^{-C't'/\eta(\text{effective})} \times e^{-\pi[N_s^0 U^2 t'^2 + I_s U^2 t'^3/3]}\, dt' \quad (1d)$$

$$H = \frac{H'}{1-f} = \frac{1}{(1 + f4G_c/3K_m)} \quad (1e)$$

$$\frac{4G_c}{3K_m} = 4\left(\frac{\eta_{eff}}{2(1+\nu_c)}\right)\left(\frac{1-2\nu_m}{\eta}\right) = \frac{2(1-2\nu_m)}{1+\nu_c}\left(\frac{\eta_{eff}}{\eta}\right) \quad (1f)$$

$$\eta(\text{effective}) = \eta e^{-2.5f/(1-af)} \quad (1g)$$

where $N_s{}^0$ is the density of surface nucleation sites at $t = 0$, I_s is the surface nucleation rate, and $U(T)$ is the crystal growth rate. H' is the linear shrinkage rate of the composite relative to the linear shrinkage rate of the glass matrix, and η(effective) is the effective viscosity of the composite. H' and η(effective) are introduced as proposed by Scherer,[9,22] f is the fiber volume fraction, G_c is the shear viscosity of the composite, η the bulk viscosity of the matrix, and ν_m and ν_c are Poisson's ratios of the matrix and composite, respectively. Since ν_m and ν_c depend on the matrix density, a first calculation of densification kinetics was carried out by approximating G_c/K_m by η(effective)/η, and then followed by an iteration using ν_m and ν_c as functions of the matrix density, as proposed by Scherer.[9] The quantity a in Eq. (1g) varies between 1 and 2. In this work, the best fit was found with $a = 2$. H has a retarding effect on the sintering kinetics because of the hydrostatic tensions generated by the inclusions, but η(effective) also has a retarding effect in the last sintering stages.

In the early stages of sintering, the system is composed of *particles* and interconnected porosity; however, at the end of the process, the system consists of isolated pores with a pore size distribution that depends on the initial particle size distribution and packing.

In the following sections, we present a new approach for modeling the sintering behavior of crystallizing glass powders containing rigid inclusions. This new approach is an extension of the *Clusters* model, and is based on an analysis that classifies the type of contacts between pairs of particles: glass–glass, fiber–fiber, or glass–fiber. This special case is important for the design and development of glass or glass–ceramic matrix/fiber composites.

II. Experimental Procedure

A borosilicate glass with composition $60SiO_2 \cdot 24B_2O_3 \cdot 16Na_2O$ mole% (SiBNa403) was used in this study. The batch was prepared from silica sand, reagent grade Na_2CO_3, and vitreous B_2O_3. The glass was melted in air in a Pt crucible, at 1500°C for 1 h. After melting, the glass was milled and sieved to obtain three different particle sizes, herewith fractions denominated as A, B, and C. The particle size distributions corresponding to these powder fractions were determined by the laser-scattering method (Mastersizer S, Malvern Instruments Ltd., Malvern, U.K.). The specific surface area was measured by BET (Monosorb Surface Area Analyzer MS-13 of Quantachrome, Boynton Beach, FL).

Commercial stabilized zirconia fibers (8 wt% yttria) with average length, 1.6 mm, and diameter, 3–6 μm, were used for the preparation of the composite. Borosilicate glass powders of different particle sizes were mixed with the zirconia fibers in different proportions in acetone for 2 h using a Turbula Mixer (System Schatz from Willy A. Bachofen AG, Basel, Switzerland). The fibers and the glass powder were previously treated in ultrasound for a few minutes to minimize the formation of agglomerates.

Cylindrical samples (height ≈ 1 cm and diameter ≈ 0.8 cm) were prepared from different mixtures by isostatic pressing at 200 MPa for 1 min. The samples were weighted and their dimensions were measured.

The compacts were isothermally treated in an electric furnace in air at 625° and 650°C during different times ($T_g = 565$°C). The densities of the green and treated samples were measured by the Archimedes method using Hg. The sintering process was analyzed for density changes and dimensional modifications of the samples.

The microstructures of the treated samples were observed by scanning electron microscopy with a Zeiss-DSM 950 microscope (Carl Zeiss, Oberkochen, Germany).

For the glass–zirconia composite, the theoretical density was calculated from the rule of mixtures:

$$\rho_{th} = \sum V_i \rho_i \quad (2)$$

where ρ_{th} is the theoretical sample density, V_i is the volume fraction of phase i, and ρ_i is its theoretical density.

The viscosity–temperature curve of the glass was determined by the rotation method for viscosities in the range 1–10^4 Pa·s, and by the fiber elongation method for viscosities in the range 10^7–10^{12} Pa·s.[14] The measurements were performed with a high-temperature viscometer (Haake, Waltham, MA) that allows the combination of both methods using a Sensor System HE 1700.

A quantitative study of the glass surface crystallization was performed. Pieces of the original glass with polished surfaces were heat treated at 650° and 700°C for different lengths of time in an electrical furnace with a thermal stability of ±2°C. Subsequently, the glasses were analyzed for crystals on the surfaces in an optical microscope (Zeiss Axioskop). The sizes of the largest isolated crystals were measured after sequential heat treatments at the temperatures listed above. Crystal growth rates, $U(T)$, were obtained from these measurements. The average numbers of crystals per unit area (N_s) were also determined.

III. Calculations

A rough estimate of the pore size among particles, in the absence of fibers, can be made considering that the particles are spherical and that part of them is in simple cubic arrangement, the remaining particles being arranged in a body-centered cubic packing (bcc). One can find[20] that the pore radius a_0 is related to the particle radius r, i.e. $a_0 \approx 0.5r$ for simple cubic and $a_0 \approx 0.2r$ for bcc arrangements. If one adds fibers to this porous compact, two different cases can be considered: (1) when the fiber diameter is greater than the pore size among the glass particles, and (2) when the fiber diameter is less than the pore size among the glass particles. Since we are dealing with a pore-size distribution, we refer to the average fiber diameter and average pore size. In this paper, we worked with a unique size distribution of fiber diameters and with three different particle size distributions: A, B, and C. While the composites formed by particles of size distribution A+fibers and particles of size distribution B+fibers are included in case (2), size distribution C+fibers correspond to case (1).

(1) Fiber Diameter > Pore Size Among the Glass Particles

In this case, the fibers cannot reside in the pores of the compact. One can then imagine that glass particles surround the fibers

generating a number of glass–fiber contacts, as well as glass–glass and fiber–fiber contacts. In what follows, we analyze the densification kinetics of each type of contact.

The classical study of Frenkel describes the first stages of sintering as the shortening of the distance between the centers of two glass particles, resulting in a decrease in the total surface area.[23] During this process, necks form between the particles, where, initially, there was only physical contact. The driving force for sintering is the decrease in surface energy.

For typical glass sintering temperatures, which are somewhat above the glass transition temperature, T_g, but well below the melting point of the zirconia fibers, we expect only three types of contact (Fig. 1): glass–glass, glass–fiber, fiber–fiber. Glass–glass contacts behave as Frenkel described, with sintering occurring through viscous flow. In contacts of the glass–fiber type, there is no possibility for the fiber to change its shape (since it is rigid at the typical sintering temperatures). The glass may or may not wet the zirconia fibers but, if so, the sintering kinetics are typically slower. This has been observed by electron microscopy of sample sections, where the remaining porosity after partial sintering was mainly associated with the fiber surfaces.[14]

Fiber–glass and fiber–fiber contacts may then be considered as frozen, since they do not evolve during sintering of the glassy phase. Based on the above considerations and the scheme of Fig. 2, three different volumes can be idealized in the composite: G, G', and F.

G is the volume distributed along the sample that exhibits only *glass–glass* contacts. It consists entirely of glassy particles with total volume g and the corresponding pores with total volume $\breve{\mathbf{g}}$, so that $G = g + \breve{\mathbf{g}}$.

In the same way, G' is the volume of glass particles that make contact with fibers (*glass–fiber* contacts). G' is composed of glass particles of total volume g' and pores with a total $\breve{\mathbf{g}}'$; $G' = g' + \breve{\mathbf{g}}'$. G' can be estimated as the product of the fiber surface areas times the average particle radius. Since glass–fiber contacts do not change with time in our sintering conditions, the relative density of this particular volume is constant and approximately equal to 0.6 in the present case.

Finally, F is the volume of the fibers. For diluted systems, the fibers are dispersed and the density of the volume they occupy is that of their constituent material, which is constant. The zirconia density is 6.09 g/cm^3 (for cubic phase). For systems with a volume fraction of fibers larger than ca. 9%, we found experimentally that fiber clusters appear along with pores, thereby decreasing the density of these regions, such that $F = f + \breve{\mathbf{f}}$, where f is the solid volume of fibers and $\breve{\mathbf{f}}$ is the volume of pores in the fiber clusters.

With the available data for each sample: mass of glass, m_g, mass of fiber, m_f, glass density, ρ_g, fiber density, ρ_f, relative green density of the compact, having initial relative density of the glassy regions (G and G'), $\rho_0 \approx 0.6$, it is possible to estimate the volumes $\breve{\mathbf{g}}$, $\mathbf{g}'$, $\breve{\mathbf{g}}'$, and $\breve{\mathbf{f}}$ of the green composite compact.

The initial value of G is calculated with Eqs. (3) and (4), at time = 0, where $2/r_f$ is the surface area per unit volume of the cylindrical fibers, and r_p is the average value of the radii of the glass particles that surround the fibers.

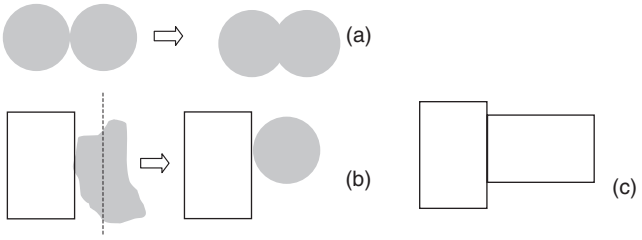

Fig. 1. Particle shape evolution during sintering. Solid gray particles represent glass particles, and white particles represent fibers. (a) Glass–glass contacts. (b) Schematic example of inclusion–glass contacts. The inclusion is rigid and the glass particle spheroidizes because of its surface tension. (c) Inclusion–inclusion contact. There is no evolution of the geometry with time.

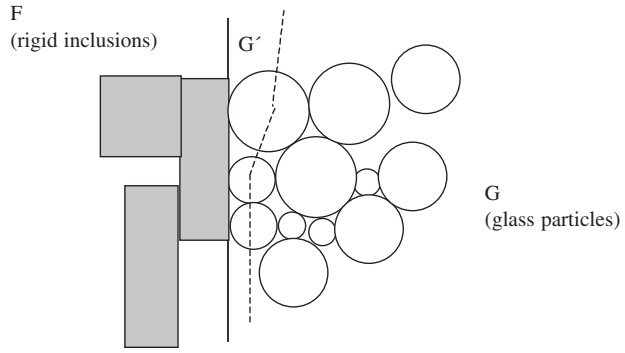

Fig. 2. Scheme example of the three different volumes (G, G', and F) considered during sintering. G contains only glass–glass contacts, G' includes rigid inclusion–glass contacts, F = volume of the fibers.

$$G + G' + F = 1 \tag{3}$$

$$G' = \left[\frac{2r_p}{r_f} + \left(\frac{r_p}{r_f}\right)^2\right] f(1 - F) \tag{4}$$

Equation (3) states that at time = 0 all the volumes G, G', and F are volume fractions, and is valid only for $t = 0$. Equation (4) estimates the volume G' as an annular volume surrounding the fibers times the probability $(1-F)$ of this volume to be glass powder. Equation (4) is derived from geometrical considerations.

The evolution of the relative density of the composite, $\rho_c(t)$, is calculated as follows:

$$\begin{aligned}\rho_c(t) &= [\text{sample mass/sample volume } (t)]/\rho_{th} \\ &= [(g + g' + f)/(G + G' + F)]\end{aligned} \tag{5}$$

Within this approximation, the volumes g', G', f, and F are constant. The evolution of the composite density is, therefore, because of the shrinkage of the sample volume that only exhibits glass–glass contacts (G).

From Eq. (1g) can be calculated as a function of time, as

$$G(t) = g[\rho(0)/\rho(t)] \tag{6}$$

The *Clusters* model is then used to calculate $\rho(t)$, the density of the glass regions. Surface crystallization kinetics were taken into account in the present calculations by introducing the measured surface density of nucleation sites (N_s) and crystal growth rate (U) in Eqs. (1c) and (1d).

(2) Fiber Diameter < Pore Size Among Glass Particles

If the average fiber diameter is less than the average pore size, we can assume that the fibers are accommodated inside the pores. Even large fibers can occupy a series of interconnected pores. In the initial stages of sintering, the glass particles near the fibers approach the fiber surface. However, at this stage no strong effect on the sintering kinetics is expected because there are few fiber–glass contacts. Once the pores contract sufficiently, the glass particles touch the fibers, generating glass–fiber contacts as described in Section III*(1)*. We consider that these contacts do not change; an associated porosity therefore appears around the fibers.

Thus, in case Section III*(2)*, the model is the same as that of Section III*(1)* but with the difference that the volume remaining with unaltered green density is now defined by the fiber radius, as Fig. 3 suggests.

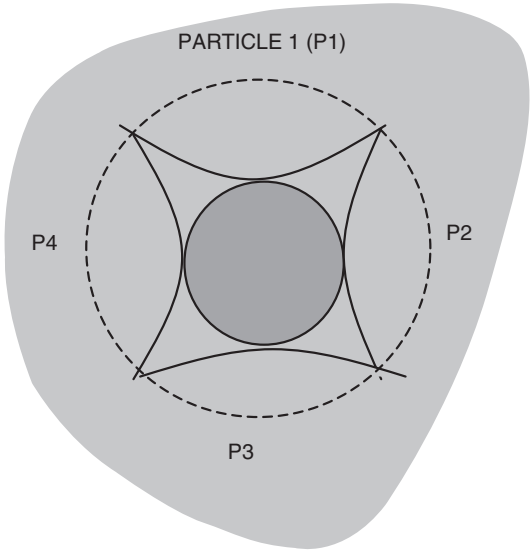

Fig. 3. Cross-section with the surfaces from particles 1, 2, 3, and 4, touching the fiber surface during pore shrinkage (at the center of the figure, the circular cross-section of the fiber). Four triangular pore sections are defined. The dashed line and the fiber contour define an annular area approximately three to four times that of the fiber cross-section.

IV. Results and Discussion

(1) Glass and Green Sample Characterization

The viscosity–temperature curve of the original glass was measured by a high-temperature viscometer.[14] Data fitting resulted in the following VFT equation, where the viscosity η is in Pa · s, and the temperature T is in K:

$$\log \eta = -4.33 + \frac{4302}{T - 545} \tag{7}$$

However, in the calculations, the viscosity was considered as an adjustable parameter. It should be stressed that only a single value of viscosity was adjusted for five different sintering experiments at 625°C, and another for six different sintering experiments at 650°C. The viscosity of the original glass is likely to be affected by the possible dissolution of Zr near the fibers, and by non-stoichiometric crystallization of the glass causing compositional changes.[14,24] We will then compare the fitted values with those calculated by Eq. (7).

Figure 4 shows the particle size distributions of the three fractions (A, B, and C) for SiBNa403 glass. The average diameter (d_{50}) and the specific surface area (S_{BET}) for the three particle-size fractions of the different glasses are presented in Table I. Fraction A (20–40 μm) of SiBNa403 glass presents a monomodal size distribution with a medium particle size diameter of ~36 μm. Fractions B and C show multimodal distribution ranging between 1–40 and 1–10 μm for B and C, respectively.

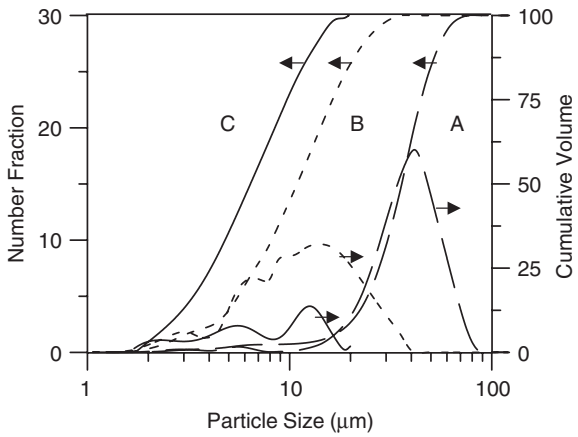

Fig. 4. Particle size distribution of the three powder fractions A, B, and C for SiBNa403 glass.

Table I. Medium Particle Size and Specific Surface Area

	SiBNa403	
Fraction (μm)	d_{50} (μm)	S_{BET} (m^2/g)
20–40 (A)	35.9 ± 0.5	0.19 ± 0.05
<20 (B)	10.9 ± 0.5	0.72 ± 0.05
<20 (C)	6.3 ± 0.5	1.90 ± 0.05

The nominal density of the (fully dense) composite was calculated from the mass densities of the SiBNa403 glass (2.46 g/cm^3) and cubic zirconia (6.09 g/cm^3) using the rule of mixtures (Eq. (2)). The fiber volume fractions ($f/[f+g]$) used were: 0.09

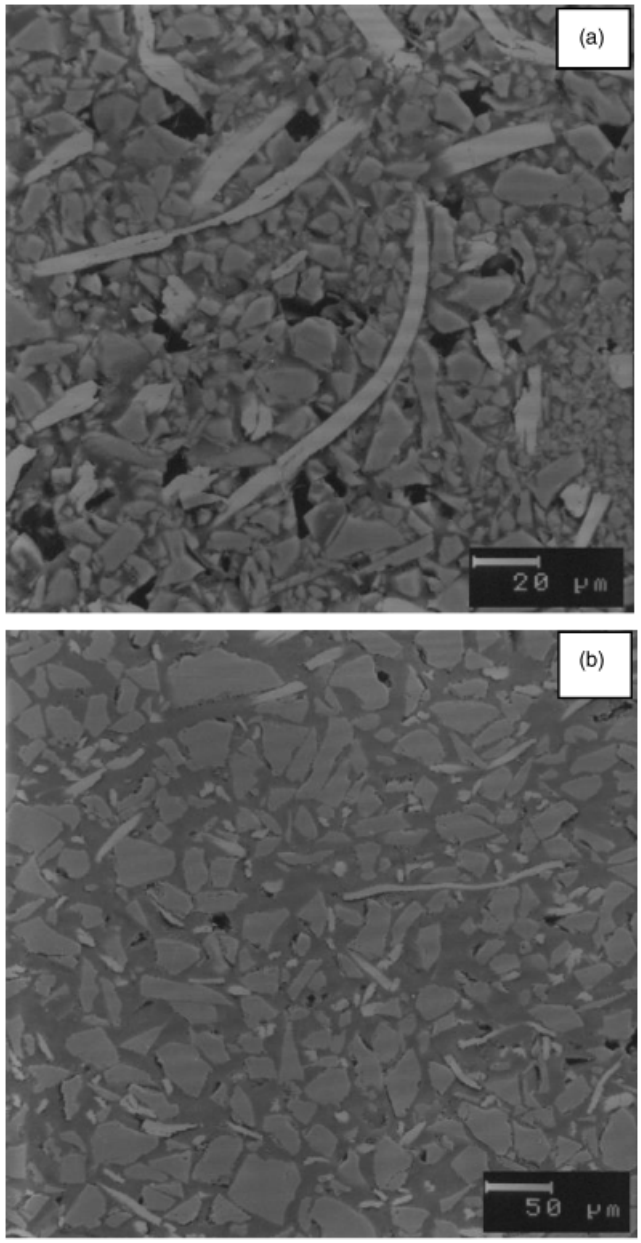

Fig. 5. Scanning electron microscopy micrographs corresponding to green composite obtained from fraction C, $f = 0.09$ (a) and from fraction A, $f = 0.09$ (b).

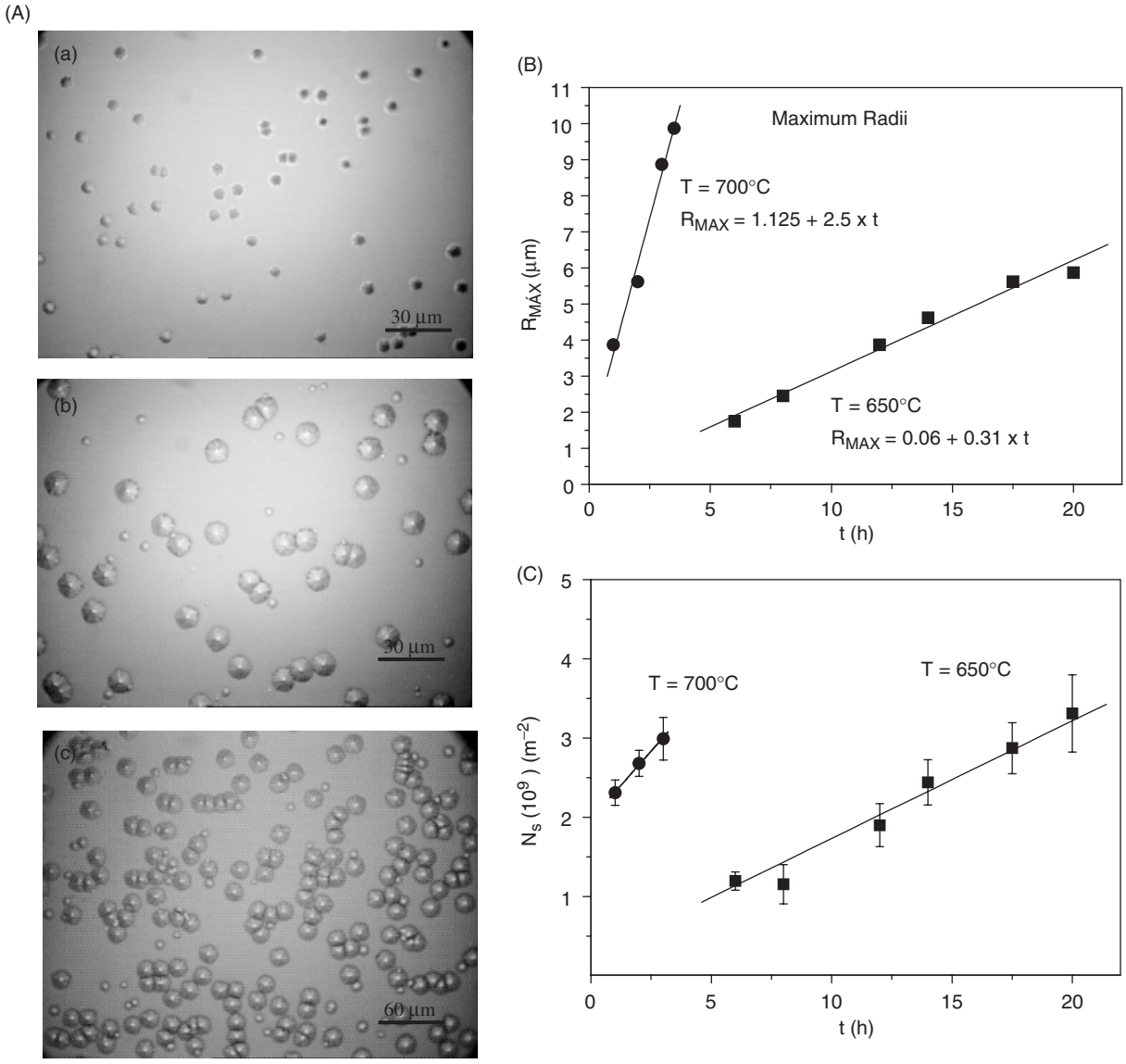

Fig. 6. (a) Partially crystallized surface after 1 h (a), 2 h (b), and 3 h (c) of thermal treatment at 700°C. (b) Measured maximum radii. (c) Density of nucleation sites.

(9 vol%, 20 wt%), 0.21 (21 vol%, 40 wt%), 0.38 (38 vol%, 60 wt%) and 0.62 (62 vol%, 80 wt%). For example, for a volume fraction, 0.09, the calculated density of the composite is 2.79 g/cm^3.

Figure 5(a) shows a micrograph of a green composite obtained from fraction C glass powders and a fiber volume fraction equal to 0.09. As described in the model, when the fiber diameter is greater than the pore size among glass particles, some particles surround and contact the zirconia fibers, reducing porosity. In contrast, Fig. 5(b) shows the case of fiber diameter less than pore size. In this case, fibers "swim" in the vast porosity left by the glass particles (darker areas), minimizing the number of fiber–glass particle contacts.

(2) Density of Nucleation Sites (N_s) and Crystal Growth Rate (U)

Figure 6(a) displays a partially crystallized surface after 1, 2, and 3 h of heat treatment at 700°C. Data shown in Figs. 6(b) and (c) were obtained from similar micrographs.

Figure 6(b) shows the measured values of the maximum crystal radii for sequential heat treatments at each temperature. We consider the crystal size to be practically zero at zero time. Figure 6(c) shows a density of nucleation sites at zero time, and a surface nucleation rate at each temperature.

The crystal growth rate at 625°C was calculated assuming linear behavior of $\ln(U)$ versus $1/T$ in the narrow temperature range used. Similarly, the surface nucleation rate at 625°C was also estimated by considering it as a thermally activated process where $\ln(N_s)$ is proportional to T^{-1}.

(3) Sintering Kinetics of the Glass Powders with Embedded Fibers

Figure 7 shows the relative density, ρ, as a function of sintering time at 625°C for the glass powder corresponding to the smallest particle size, fraction C, containing different volume fractions of ZrO_2 fibers. The sintering behavior of the fiber-free glass ($f = 0$) is also presented for the same particle size distribution. The glass compacts ($f = 0$) sinter to a relative density of 0.98 after 5 h, while the maximum densification reached for composites with a fiber volume fraction equal to 0.09 is 0.94 after 24 h of treatment. Densification is greater for smaller fiber contents.

The curves in Fig. 7 were obtained by calculation using the modified *Clusters* model. The parameters used for calculating all curves of Fig. 7 are: $\eta = 10^{9.1}$ Pa · s (the experimental, VFT fitted value, was $10^{7.85}$ Pa · s), $N_s = (0.1 \times 10^9 + 25530 \times \text{time})$ m^{-2} (measured value, time in seconds), and $U = 0.146 \times 10^{-10}$ m/s (measured value). We remark that these values have been used for all the calculated kinetics, and that the measured saturation

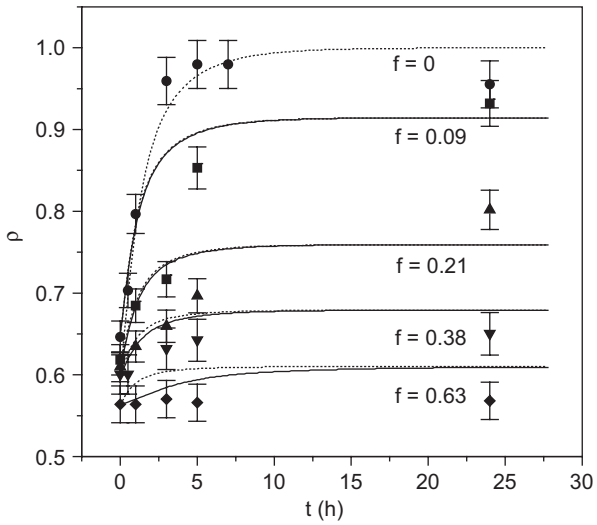

Fig. 7. Experimental points and theoretical curves corresponding to the sintering kinetics of fraction C with different fiber contents at 625°C. Solid lines correspond to calculations taking into account tensions generated by inclusions; dotted lines: without tensions.

densities are predicted by the model. While the saturation density depends on the glass volume fraction that is allowed to sinter (one should recall that a thin layer of glass powder in contact with the fiber surface is not allowed to sinter), the sintering rate is strongly affected by the tensions created by the inclusions. In the same figure, we show the calculated sintering kinetics, with and without hydrostatic tensions. In summary, larger volume fractions of inclusions result in slower sintering kinetics and larger porosity, or smaller relative density at saturation.

While viscosity affects the sintering kinetics in both Frenkel and MS stages, the empirical shape factor only impacts on the Frenkel stage. N_s and U slow down the sintering kinetics and determine the saturation density, especially in those cases where there is strong competition between crystallization and sintering. As shown above, besides the fiber content, the influence of crystallization has also been considered. Nevertheless, in this case, the fiber content is the strongest limiting factor of densification. This is so because the volume G' that will not sinter is proportional to the fiber content.

Discrepancies between calculations and experiments, which are mainly observed for large fiber contents, may be because of the formation of isolated clusters of glass particles that are surrounded by fibers (Fig. 8). Although shrinkage may occur within these clusters, this does not result in sample shrinkage.

In a "diluted" system, the fibers do not interact with each other. However, when the fiber content increases, contacts among fibers increase. In the case of long fibers (fiber length of approximately 1.6 mm, maximum glass particle size in the range 0.001–0.1 mm), a fiber network is formed with internal glass powder regions, which sinter almost independently from

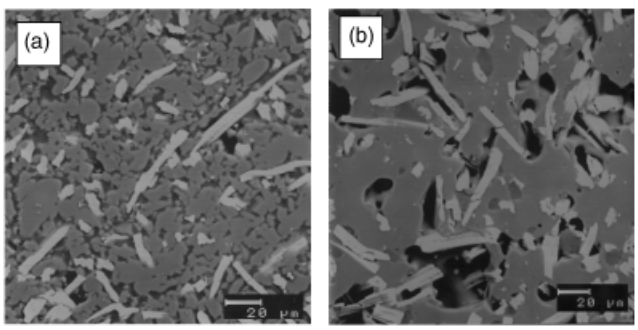

Fig. 8. Scanning electron microscopy micrographs corresponding to fraction C, $f = 0.21$ at 625°C during 3 h (a) and during 24 h (b).

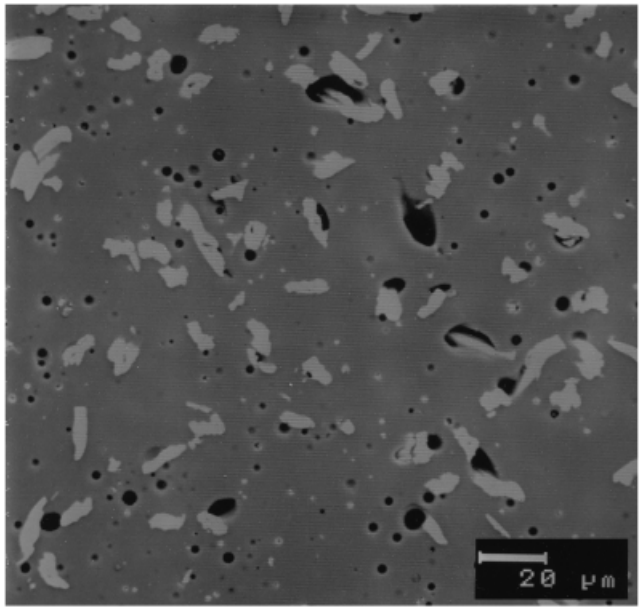

Fig. 9. Scanning electron microscopy micrograph corresponding to fraction C, $f = 0.09$ at 625°C during 24 h.

each other. Stresses imposed by the glass on the strong fibers during sintering are not sufficient to deform this network. For instance, at a fiber volume fraction of about 0.65, no shrinkage was observed by Pascual *et al.*[14]

To obtain composite densities higher than 80% in this temperature range, the maximum fiber fraction should be $f \sim 0.09$ (Fig. 9). A densification study at 650°C with samples of different particle size and this fiber content is described below.

Figures 10(a)–(c) show the sintering kinetics of mixtures of SiBNa403 glass with 9 vol% ZrO_2 fibers ($f = 0.09$) treated at 650°C for the three particle sizes, compared with the corresponding glass ($f = 0$). Dots refer to experimental data and continuous curves refer to the calculated sintering kinetics using the modified *Clusters* model.

The viscosity of the original glass at this temperature is log $\eta = 7.05$ (η in Pa · s). The maximum relative density for SiBNa403 glass ($\rho = 0.98$) is reached after 5, 3, and 0.5 h for treatment with powders of fraction A, B, and C, respectively. Once the maximum density is reached, longer treatment times lead to a decrease of the density for all the particle size distributions because of quartz crystallization, which leads to degassing and the appearance of porosity.[14]

As expected, a maximum density of 0.94 is reached after 3 h at 650°C for the mixture of ZrO_2 fibers with the glass powder of the smallest particle size (fraction C), Fig. 10(c).[19] When larger particle sizes are used, around 5 h are necessary to reach a maximum relative density of $\rho = 0.84$, indicating that the increase of the glass particle size along with ZrO_2 fibers inhibits complete densification.[1]

The parameters used for the calculation of the curves in Fig. 8 are: $\eta = 10^{8.35}$ Pa · s (fitted value) compared with a measured value of $10^{7.05}$ Pa · s, $N_s = (0.2 \times 10^9 + 41280 \times \text{time})$ m^{-2} (measured value, time in seconds), $U = 0.86 \times 10^{-10}$ m/s (measured value).

A problem with the present analysis is that the fitted values of viscosity include a series of chemical and physical phenomena. Regarding chemical phenomena, the viscosity of the original glass is likely to be affected by the possible dissolution of Zr near the fibers, and by non-stoichiometric crystallization of the glass causing compositional changes.[14,24] In terms of physical effects, the unknown shape factor, k_s, of the irregular particles, and the irregular packing of the glass particles results in $p_f < 1$ (p_f, number of neighbors per particle), but its real value is unknown. Therefore, the unknown product of these two quantities ($k_s p_f$) is included in the fitted viscosity values. The complex sum of all

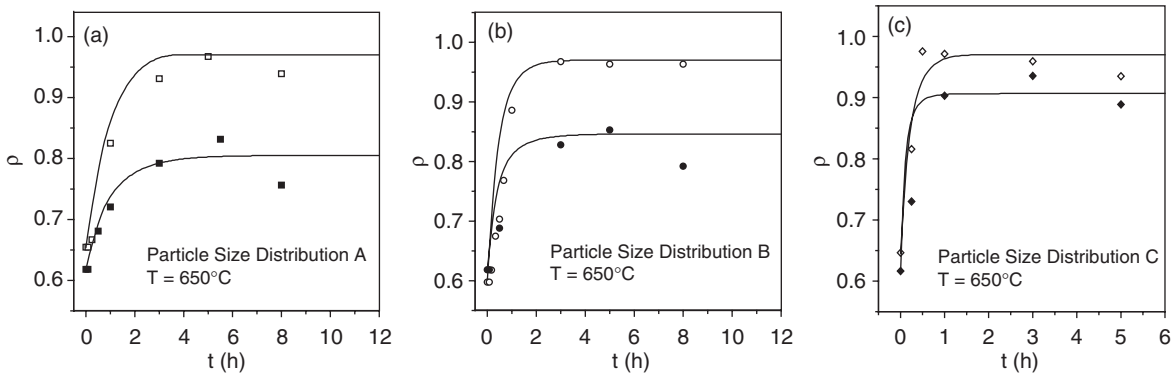

Fig. 10. (a) Experimental points (hollow: without fibers, solid: with 0.09 fiber volume fraction) and theoretical curves corresponding to the sintering kinetics of particle size distribution A with 0 and 0.09 volume fraction fiber content. (b) Idem for particle size distribution B. (c) Idem for particle size distribution C.

these effects results in fitted viscosity values that are approximately one order of magnitude as great as the measured viscosity of the original parent glass. However, it should be stressed that only one viscosity was fitted for each temperature.

Bubble formation occurs because of degassing of the glass particles during sintering. This phenomenon may or may not be connected to crystallization, but it is not considered in the sintering models,[14] and is possibly a source of discrepancy between calculated and experimental data at longer times when the sample is crystallizing.

Figures 10(a)–(c) show that reasonable agreement is found between calculations and experiments for size distribution C (fiber diameter $\gg$ pore size). The model also describes the sintering kinetics for size distributions A and B (fiber diameter $<$ particle size).

The advantages of the extended *Clusters* model rest in its ability to correctly predict trends in sintering kinetics and saturation density as a function of particle size distribution, fiber diameter, and sintering temperature, with or without simultaneous crystallization. However, as for other models, it does not consider the effect of degassing and possible chemical reactivity between the glass matrix and inclusions.

From the present results, it is evident that to reduce the final porosity, the volume G' must be reduced. This condition is met by, for example, decreasing the glass particle size. Additional experiments could include coating of the inclusions with a suitable glaze that would eliminate inclusion-glass contacts, thus decreasing G'.

The present model can also be useful in the case of two different glasses sintered together, in the case where the viscosity of one glass is much larger than the other at the sintering temperature and thus behaves as a rigid inclusion.

V. Conclusions

We extended the *Clusters* model for sintering powdered glasses undergoing simultaneous surface crystallization to take into account the existence of rigid fibers with different fiber diameter/pore size ratios embedded in a glass powder matrix. We then successfully tested this modified *Clusters* model with the sintering kinetics of borosilicate glass/zirconia fiber composites and proved that it is an alternative to other successful sintering models. The main advantage of the extended *Clusters* model is that it takes into account important parameters, such as the glass particle size distribution; the dimensions, volume fractions, and hydrostatic tensions generated by the inclusions; and simultaneous surface crystallization.

Acknowledgments

The careful review by Eduardo B. Ferreira of LaMaV-UFSCar (Brazil) is deeply appreciated. Thanks are also due to CNPq, Fapesp, and Pronex (Brazil).

References

[1]F. F. Lange, D. C. C. Lam, and O. Sudre, "Powder Processing and Densification of Ceramic Composites"; pp. 309–18 in *Processing Science of Advanced Ceramics*, Edited by I. S. Aksay, G. L. McVay, and D. R. Ulrich. Materials Research Society, Pittsburgh, PA, 1989.

[2]A. G. Evans, "Considerations of Inhomogeneity Effects in Sintering," *J. Am. Ceram. Soc.*, **65**, 497–501 (1982).

[3]R. Raj and R. K. Bordia, "Sintering Behaviour of Bimodal Compacts," *Acta Metall.*, **32**, 1003–19 (1984).

[4]C. H. Hsueh, A. G. Evans, R. M. Cannon, and R. J. Brook, "Viscoelastic Stresses and Sintering Damage in Heterogeneous Powder Compacts," *Acta Metall.*, **34**, 927–36 (1986).

[5]C. H. Hsueh, A. G. Evans, and R. M. McMeeking, "Influence of Multiple Heterogeneities on Sintering Rates," *J. Am. Ceram. Soc.*, **69**, C-64–6 (1986).

[6]M. N. Rahaman and L. C. De Longhe, "Effect of Rigid Inclusions on the Sintering of Glass Powder Compacts," *J. Am. Ceram. Soc.*, **70**, C-348–51 (1987).

[7]R. E. Dutton and M. N. Rahaman, "Sintering, Creep, and Electrical Conductivity Model Glass–Matrix Composites," *J. Am. Ceram. Soc.*, **75**, 2146–54 (1992).

[8]A. R. Boccaccini, "Sintering of Glass Matrix Composites Containing Al_2O_3 Platelet Inclusions," *J. Mater. Sci.*, **29**, 4273–8 (1994).

[9]G. W. Scherer, "Sintering with Rigid Inclusions," *J. Am. Ceram. Soc.*, **70**, 719–25 (1987).

[10]G. W. Scherer, "Viscous Sintering of a Bimodal Pore Size Distribution," *J. Am. Ceram. Soc.*, **67**, 709–15 (1987).

[11]G. W. Scherer, "Viscous Sintering with a Pore-Size Distribution and Rigid Inclusions," *J. Am. Ceram. Soc.*, **71**, C-447–8 (1988).

[12]P. C. Panda, W. M. Mobley, and R. Raj, "Effect of the Heating Rate on the Relative Rates of Sintering and Crystallization in Glass," *J. Am. Ceram. Soc.*, **72** [12] 2361–4 (1989).

[13]P. C. Panda and R. Raj, "Sintering and Crystallization of Glass at Constant Heating Rates," *J. Am. Ceram. Soc.*, **72** [8] 1564–6 (1989).

[14]M. J. Pascual, A. Durán, and L. Pascual, "Sintering Behavior of Composite Materials Borosilicate Glass–ZrO_2 Fibre," *J. Eur. Ceram. Soc.*, **22**, 1513–24 (2002).

[15]G. W. Scherer, "Sintering of Low-Density Glasses: I, Theory," *J. Am. Ceram. Soc.*, **60**, 236–9 (1977).

[16]M. O. Prado, E. D. Zanotto, and R. Müller, "Model for Sintering Polydispersed Glass Particles," *J. Non-Cryst. Solids*, **279** [2–3] 169–78 (2001).

[17]E. D. Zanotto and M. O. Prado, "Isothermal Sintering with Concurrent Crystallization of Monodispersed and Polydispersed Glass Particles. Part I," *Phys. Chem. Glasses*, **42** [3] 191–8 (2001).

[18]M. O. Prado, C. Fredericci, and E. D. Zanotto, "Isothermal Sintering with Concurrent Crystallization of Polydispersed Soda–Lime–Silica Glass Beads," *J. Non-Cryst. Solids*, **331** [1–3] 145–56 (2003).

[19]M. O. Prado, C. Fredericci, and E. D. Zanotto, "Non-Isothermal Sintering with Concurrent Crystallization of Polydispersed Soda–Lime–Silica Glass Beads," *J. Non-Cryst. Solids*, **331** [1–3] 157–67 (2003).

[20]M. O. Prado, E. D. Zanotto, and C. Fredericci, "Sintering Polydispersed Spherical Glass Particles," *J. Mater. Res.*, **18** [6] 1347–54 (2003).

[21]M. O. Prado, C. Fredericci, and E. D. Zanotto, "Glass Sintering with Concurrent Crystallization Part II. Non-Isothermal Sintering of Jagged Polydispersed Particles," *Phys. Chem. Glasses*, **43** [5] 215–23 (2002).

[22]G. W. Scherer, "Effect of Inclusions on Shrinkage"; pp. 503–14 in *Better Ceramics Through Chemistry*, **Vol. IV**, Edited by B. J. J. Zelinski, C. J. Brinker, D. E. Clark, and D. R. Ulrich. Materials Research Society, Pittsburgh, PA, 1990.

[23]J. Frenkel, "Viscous Flow of Crystalline Bodies Under the Action of Surface Tension," *J. Phys. (USSR)*, **IX** [5] 385 (1945).

[24]M. J. Pascual and A. Durán, "Sintering with Concurrent Crystallization of a Borosilicate Glass," *Phys. Chem. Glasses*, **44** [6] 409–15 (2003). □